



## 4-Hydroxycoumarin Derivatives as Corrosion Inhibitors for Copper in Nitric Acid Solutions

A.S. Fouda<sup>1</sup>, S.M. Rashwan<sup>2</sup>, M.M. Kamel<sup>2</sup> and M.M. Khalifa<sup>1</sup>

<sup>1</sup>Department of Chemistry, Faculty of Science, El-Mansoura University, El-Mansoura-35516, Egypt:email:

<sup>2</sup>Department of Chemistry, Faculty of Science, Suez Canal University. Egypt.

Received 01 Dec 2015, Revised 09 Apr 2016, Accepted 16 Apr 2016

\*Corresponding author. E-mail: [asfouda@mans.edu.eg](mailto:asfouda@mans.edu.eg); Fax: +2 050 2246254 Tel: +2 050 2365730.

### Abstract

The corrosion behavior of copper in 1M HNO<sub>3</sub> and in the presence of 4-hydroxycoumarin derivatives has been investigated using, electrochemical impedance spectroscopy (EIS), potentiodynamic polarization, electrochemical frequency modulation (EFM) and weight loss techniques. Results of EIS showed the increase in the charge transfer resistance and the decrease in the double layer capacitance. Polarization studies showed that, these compounds act as mixed- type inhibitors. Inhibition efficiency of these compounds has been found to vary with concentration of the 4-hydroxycoumarin derivatives and temperature. The adsorption of these compounds on the surface of copper from the acid solution has been found to obey Temkin adsorption isotherm. The thermodynamic activation parameters of copper corrosion in 1M HNO<sub>3</sub> were determined and discussed. The results obtained from all tested techniques were in good agreement.

**Keywords:** Copper corrosion, 4-hydroxycoumarin derivatives, HNO<sub>3</sub>, Temkin isotherm

### 1. Introduction

Copper has an excellent electrical and thermal conductivities, good corrosion resistance and mechanical workability. It is widely used in heating and cooling systems. Corrosion of copper can lead to many problems, the most being perforation that may result in coolant leakage. Scales and corrosion products have negative influence on heat-transfer, causing a decrease in heating efficiencies of the copper structures [1]. Thus, corrosion of copper and copper alloys and their inhibition in aqueous solutions have attracted the attention of a number of investigators [2]. Copper is relatively noble metal, requiring strong oxidants for its corrosion. The chemical dissolution and electroplating are the main processes used in the fabrication of electronic devices. The most widely used is nitric acid solution [3]. Corrosion inhibition of copper can be achieved through the modification of its interface by forming self-assembled ordered ultrathin layers of organic inhibitors. Efficient inhibitors for copper are heterocyclic organic compounds consisting of a  $\pi$ -system and P, S, N, or O hetero-atoms. It is noticed that presence of these functional groups and hetero-atoms in the organic compound molecules such as azoles [4], amines [5], amino acids [6], improve their action as copper corrosion inhibitor because they enable chemisorptions. Organic derivatives also offer special affinity to inhibit corrosion of various metals in different acidic media [7] and in many other solutions. Protection efficiency of organic inhibitors is attributed mainly to the presence of a polar group acting as an active center for adsorption on the metallic surface [8]. This is explained by the presence of vacant d-orbitals in copper atom that form coordinative bonds with atoms able to donate electrons. Interaction with rings containing conjugated bonds  $\pi$ -electrons is also present.

In the present study, electrochemical impedance spectroscopy (EIS) was employed which is well-established and powerful technique in the study of corrosion. Surface properties, electrode kinetics and mechanistic information can be obtained from impedance diagrams. The electrochemical frequency modulation (EFM) technique was used

as a non-linear distortion technique, evaluated as an instantaneous corrosion monitoring technique and was used here for online monitoring of corrosion rate of copper in the absence and presence of the investigated compounds. The purpose of this paper is to study the inhibition properties of 4-Hydroxycoumarin derivatives and compare the corrosion inhibition data derived from EFM with that obtained from EIS, Polarization studies and weight loss techniques. Surface morphology of copper surface was examined using scanning electron microscopy (SEM) and energy dispersive X-ray (EDX). The effect of the temperature on the rate of corrosion and thermodynamic parameters were determined and discussed.

## 2. Experimental

### 2.1. Composition of copper samples

**Table1:** Chemical composition of the copper in weight %

Element	Fe	Ni	Si	Pb	As	Cu
Weight %	0.0297	0.0103	0.0053	0.023	0.0087	The rest

### 2.2. Preparation of the inhibitors

4-hydroxycoumarin or its para-substituted derivatives (10 mmol) were dissolved in hydrochloric acid (HCl) (25mmol/25 cm<sup>3</sup> bi-distilled water). The aniline salts produced were diazotized below -5°C with a solution of sodium nitrite (80 mg, 10 mmol, 30 cm<sup>3</sup> bi-distilled water). The obtained diazonium salts were coupled with a pyridine solution of 4-hydroxycoumarin (1660 mg, 10 mmol/5 cm<sup>3</sup> pyridine). The crude dyes were collected by filtration followed by crystallized from dimethylformamide (DMF) and then dried in a vacuum desiccator over P<sub>2</sub>O<sub>5</sub> [9].

### 2.3. Chemicals and solutions

The aggressive solutions, 6 M HNO<sub>3</sub> were prepared by dilution of BDH grade (70 %) HNO<sub>3</sub> with bi-distilled water, and its concentration was checked by standardized solution of NaOH, then 1M HNO<sub>3</sub> were prepared by dilution with bi-distilled water. 100 ml stock solutions (10<sup>-3</sup> M) of every investigated compounds were prepared by dissolving an accurately weighed quantity of each material in an appropriate volume of dimethyl formamide (DMF) and absolute ethanol, then the required concentrations (5 x10<sup>-6</sup> - 30 x10<sup>-6</sup>M) were prepared by dilution with bi-distilled water. The organic inhibitors used in this study were some 4-hydroxycoumarin derivatives, as listed in Table 2.

### 2.4. Methods used for corrosion measurements

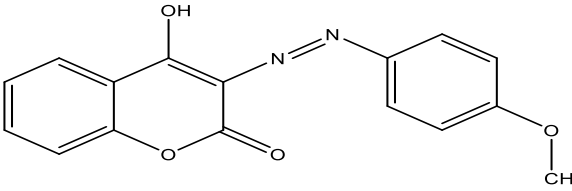
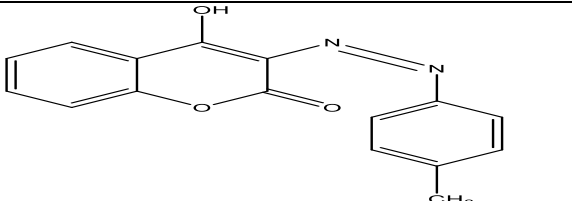
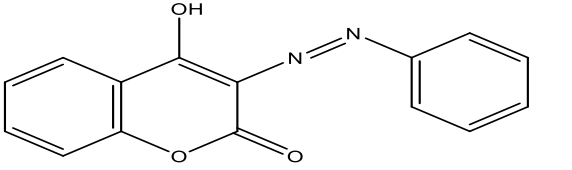
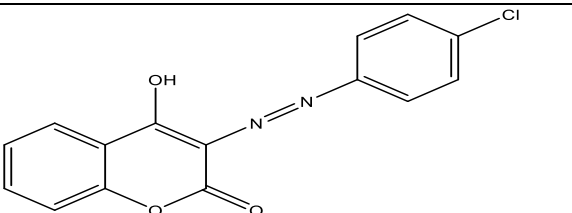
#### 2.4.1. Weight loss method

The weight loss experiments were carried out using square specimens of size 2 × 2 × 0.2 cm. The specimens were first abraded to a mirror finish using (600, 800 and 1200) grit emery papers, immersed in acetone and finally washed with bi-distilled water and dried before being weighed and immersed into the test solution. The weight loss measurements were carried out in a 100 ml capacity glass beaker, placed in water thermostat, containing 100 ml of 1 M HNO<sub>3</sub> with and without addition of different concentrations of the listed 4-hydroxycoumarin derivatives. All the aggressive acid solutions were open to air. After 6 hours of immersion the specimens were taken out, washed, dried, and weighed accurately. The average weight loss of all copper specimens could be obtained. The inhibition efficiency (% IE) and the degree of surface coverage (θ) of 4-hydroxycoumarin derivatives for the corrosion of copper were calculated as follows:

$$\% IE = \theta \times 100 = [(W^o - W) / W^o] \times 100 \quad (1)$$

where  $W^o$  and  $W$  are the values of the average weight losses in the absence and presence of the inhibitor, respectively. The values of the degree of surface coverage  $\theta$  were evaluated at different concentrations of the inhibitors in 1 M HNO<sub>3</sub> solution.

**Table 2:** Chemical structures, names, molecular weights and molecular formulae of the 4-hydroxycoumarin derivatives

Comp	Structures	Names	Mol. Formulas, Mol. Weights
A		4-hydroxy-3-(p-methoxyphenylazo)-benzopyrane-2-one	C <sub>16</sub> H <sub>12</sub> N <sub>2</sub> O <sub>4</sub> 296.28
B		4-hydroxy-3-(p-methylphenylazo)-benzopyrane-2-one	C <sub>16</sub> H <sub>12</sub> N <sub>2</sub> O <sub>3</sub> 280.28
C		4-hydroxy-3-phenylazo-benzopyrane-2-one	C <sub>15</sub> H <sub>10</sub> N <sub>2</sub> O <sub>3</sub> 266.25
D		4-hydroxy-3-(p-chlorophenylazo)-benzopyrane-2-one	C <sub>15</sub> H <sub>9</sub> N <sub>2</sub> O <sub>3</sub> Cl 300.70

#### 2.4.2. Potentiodynamic polarization method

Polarization experiments were carried out in a conventional three-electrode cell with platinum gauze as the auxiliary electrode (1cm<sup>2</sup>) and a saturated calomel electrode (SCE) coupled to a fine Luggin capillary as reference electrode. The working electrode was in the form of a square cut from copper sheet of equal composition embedded in epoxy resin, so that the exposed surface area was (1cm<sup>2</sup>). Prior to each measurement, the electrode surface was pretreated in the same manner as shown in the weight loss experiments. Before measurements, the working electrode was abraded with a series of emery papers of different grit sizes up to 1200, washed several times with bi-distilled water then degreased with acetone, finally washed several times with bi-distilled water and dried. The open circuit electrode potentials were allowed to stabilize for 30 min (until a steady state was reached) before polarizing the test electrodes from - 600 to + 400 mV vs open circuit potential (E<sub>ocp</sub>). All experiments were carried out in freshly prepared solutions at 25 ± 1°C and results were repeated at least three times to check the reproducibility.

#### 2.4.3. Electrochemical impedance spectroscopy (EIS) method

Impedance measurements were carried out using AC signals of 5 mV peak to peak amplitude at the open circuit potential in the frequency range of 100 kHz to 0.1 Hz. All the impedance data were fitted to appropriate equivalent circuit using the Gamry Echem Analyst software. The experimental impedance were analyzed and interpreted on the basis of the equivalent circuit. The inhibition efficiency (% IE) and the surface coverage (θ) of the investigated inhibitors obtained from the impedance measurements were calculated from equation (2) [10]:

$$\% IE = \theta \times 100 = [1 - (R_{ct}^{\circ} / R_{ct})] \times 100 \quad (2)$$

where  $R_{ct}^{\circ}$  and  $R_{ct}$  are the charge transfer resistances in the absence and presence of inhibitor, respectively.

#### 2.4.4. Electrochemical frequency modulation (EFM) method

EFM experiments were performed by applying potential perturbation signal with amplitude 10 mV with two sine waves of 2 and 5 Hz. The choice for the frequencies of 2 and 5 Hz was based on three arguments [11]. The larger peaks were used to calculate the corrosion current density ( $i_{corr}$ ), the Tafel slopes ( $\beta_c$  and  $\beta_a$ ) and the causality factors CF-2 and CF-3 [12].

All electrochemical experiments were carried out at  $25 \pm 1^{\circ}\text{C}$ , using Gamry instrument PCI300/4 Potentiostat/Galvanostat/Zra analyzer. DC105 corrosion software, EIS300 electrochemical impedance spectroscopy software, EFM140 electrochemical frequency modulation software and Echem Analyst 5.5 for plotting, graphing, data fitting the results and calculating

#### 2.4.5. Surface morphology

The copper surface was prepared by keeping the specimens for three hours (and 6 hrs) in 1M  $\text{HNO}_3$  in the presence and absence of optimum concentration of investigated 4-hydroxycoumarin derivatives, after abrading with different emery papers up to 1200 grit size and then polished with  $\text{Al}_2\text{O}_3$  (0.5 $\mu\text{m}$  particles size), then washed several times with bi-distilled water and with acetone then immerse it in the solution. Then the specimens were washed gently with bi-distilled water, carefully dried and mounted into the spectrometer without any further treatment. The corroded copper surfaces were examined using an X-ray diffractometer Philips (pw-1390) with Cu-tube (Cu  $\text{K}\alpha_1$ ,  $\lambda = 1.54051 \text{ \AA}$ ), a scanning electron microscope (SEM, JOEL, JSM-T20, Japan).

### 3. Results and discussion

#### 3.1. Potentiodynamic polarization measurements

Theoretically, copper can hardly be corroded in the deoxygenated acid solutions, as copper cannot displace hydrogen from acid solutions according to the theories of chemical thermodynamics [13]. However, this situation will change in nitric acid. Dissolved oxygen may be reduced on copper surface and this will allow corrosion to occur. It is a good approximation to ignore the hydrogen evolution reaction and only consider oxygen reduction in the nitric acid solutions at potentials near the corrosion potentials [14]. Nitric acid is a strong copper oxidizer capable of rapidly attacking copper. In addition, the Tafel polarization curves exhibit no steep slope in the anodic range, meaning that no passive films were formed on the copper surface. Polarization measurements were carried out in order to gain knowledge concerning the kinetics of the cathodic and anodic reactions. Figure 1 shows the polarization behavior of copper electrode in 1M  $\text{HNO}_3$  in the absence and presence of various concentrations of compound (A). Similar curves were obtained for other compounds (not shown). The values of electrochemical parameters such as corrosion current densities ( $i_{corr}$ ), corrosion potential ( $E_{corr}$ ), cathodic Tafel slope ( $\beta_c$ ), anodic Tafel slope ( $\beta_a$ ), degree of surface coverage ( $\theta$ ) and inhibition efficiency (% IE) were calculated from the curves of (Figure .1) and are listed in (Table 3) for all the investigated compounds.

The results in Table 3 revealed that both the anodic and cathodic reactions were affected by the addition of investigated organic derivatives and the inhibition efficiency increased as the inhibitor concentration increased, meaning that the addition of investigated derivatives reduced the anodic dissolution of copper and also retarded the cathodic reactions. In the presence of inhibitors  $E_{corr}$  was enhanced with no definite trend, indicating that these compounds act as mixed-type inhibitors in 1 M  $\text{HNO}_3$ , forming an adsorbed layer of these compounds at the metal/solution interface that decreased the available anodic and cathodic sites. The corrosion current density decreased obviously after the addition of inhibitors in 1 M  $\text{HNO}_3$  and % IE increased with increasing the inhibitor concentration. % IE and the degree of surface coverage ( $\theta$ ) were calculated from equation (3):

$$\% IE = \theta \times 100 = [(i_{corr} - i_{corr(inh)}) / i_{corr}] \times 100 \quad (3)$$

where  $i_{corr}$  and  $i_{corr(inh)}$  were the uninhibited and inhibited corrosion current density values, respectively.

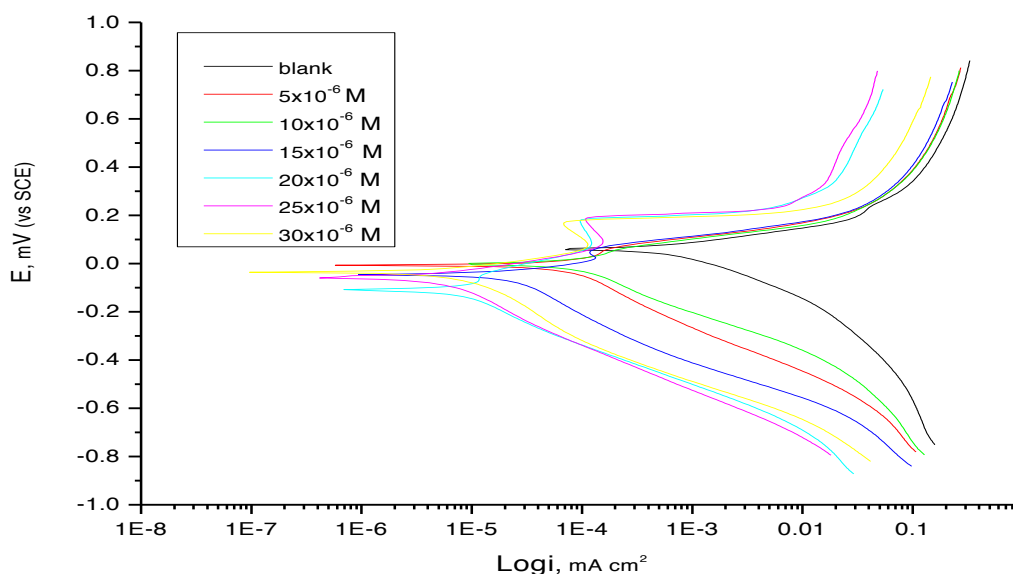


**Figure 1:** Potentiodynamic polarization curves for the corrosion of copper in 1M HNO<sub>3</sub> in the absence and presence of various concentrations of inhibitor (A) at 25°C

**Table 3:** Data from potentiodynamic polarization of copper in 1M HNO<sub>3</sub> containing various concentrations of various inhibitors at 25°C

Comp	Conc., x 10 <sup>6</sup> M	E <sub>corr</sub> , mV (vs SCE)	i <sub>corr</sub> , μA cm <sup>-2</sup>	β <sub>c</sub> mV dec <sup>-1</sup>	β <sub>a</sub> mV dec <sup>-1</sup>	C.R, Mpy	θ	% IE
Blank	0	60	768.0	192	80	740.4	----	----
A	5	17	70.8	189	82	67.54	0.907	90.7
	10	15	45.3	175	83	42.19	0.941	94.1
	15	45	38.4	184	85	35.82	0.950	95.0
	20	59	30.2	181	89	26.81	0.960	96.0
	25	58	26.9	200	105	22.28	0.964	96.4
	30	36	20.1	201	98	17.44	0.973	97.3
B	5	17	87.2	148	76	84.01	0.884	88.4
	10	14	70.1	159	87	67.07	0.908	90.8
	15	25	65.3	141	80	63.54	0.915	91.5
	20	46	49.6	164	55	47.84	0.934	93.4
	25	37	44.0	164	76	41.55	0.942	94.2
	30	21	28.5	157	58	25.54	0.962	96.2
C	5	13	100.7	136	69	97.18	0.868	86.8
	10	11	80.7	153	97	76.13	0.894	89.4
	15	45	68.2	139	78	66.42	0.911	91.1
	20	15	55.6	143	84	52.70	0.927	92.7
	25	14	49.7	148	62	47.86	0.935	93.5
	30	13	45.9	138	82	43.91	0.940	94.0
D	5	55	339.0	145	61	323.5	0.558	55.8
	10	31	336.1	146	67	326.3	0.561	56.1
	15	55	266.0	177	52	256.5	0.653	65.3
	20	57	157.2	165	43	150.8	0.795	79.5
	25	47	153.0	182	59	147.1	0.80	80.0
	30	38	136.0	156	85	130.9	0.822	82.2

As indicated from Table 3, i) the change in  $\beta_c$  values between the inhibitor-containing systems and the blank were higher than that of  $\beta_a$ , which indicated that the inhibitors predominantly inhibited cathodic reactions, even though anodic dissolution of copper was also inhibited and ii) The  $i_{corr}$  values decreased by the addition of inhibitors. Thus, addition of these inhibitors reduced the copper dissolution as well as, retarded the cathodic reaction. Thus, the adsorbed inhibitors acted by simple blocking of the active sites for both anodic and cathodic processes. In other words, the inhibitors decreased the surface area available for anodic dissolution and oxygen reduction without affecting the reaction mechanism. The order of inhibition efficiency of the investigated compounds was found to be:

$$A > B > C > D$$

### 3.2. Electrochemical impedance spectroscopy (EIS) measurements

Figure 2 shows the Nyquist plots obtained for the copper electrode at respective corrosion potentials after 30 min immersion in 1 M HNO<sub>3</sub> in the presence and absence of various concentrations compound (A) at 25°C. Similar curves were obtained for the other compounds (not shown). As the inhibitor concentration increased, the semi-circle diameter was increased. The deviation from ideal semicircle was generally attributed to the frequency dispersion as well as to the inhomogenities of the surface [15]. The EIS spectra of the investigated derivatives were analyzed using the equivalent circuit, Figure 3, which represents a single charge transfer reaction and fits well with these experimental results. The constant phase element, CPE, is introduced in the circuit instead of a pure double layer capacitor to give a more accurate fit [16]. The double layer capacitance,  $C_{dl}$ , for a circuit including a CPE parameter ( $Y^0$  and  $n$ ) was calculated from equation (4) [17]:

$$C_{dl} = Y^0 \omega^{n-1} / \sin [n (\pi/2)] \tag{4}$$

where  $Y^0$  is the magnitude of the CPE,  $\omega = 2\pi f_{max}$ ,  $f_{max}$  was the frequency at which the imaginary component of the impedance was maximum and the factor  $n$ , was an adjustable parameter that usually lied between 0.5 and 1.0.

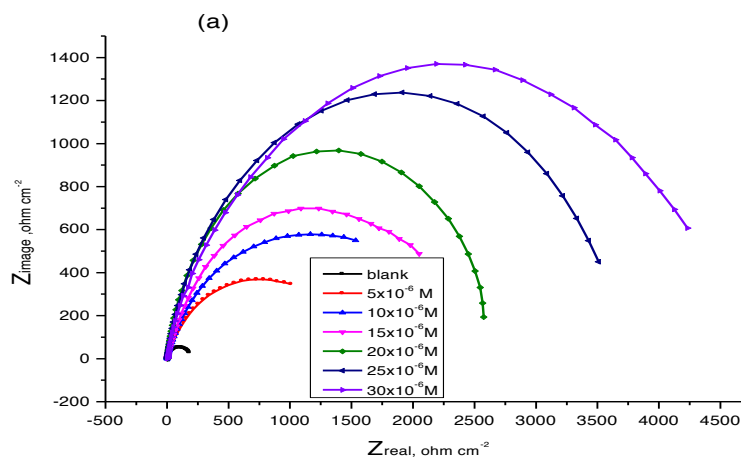


**Figure 2:** EIS Nyquist plots for copper in 1M HNO<sub>3</sub> in the absence and presence of different concentrations of compound (A) 25°C

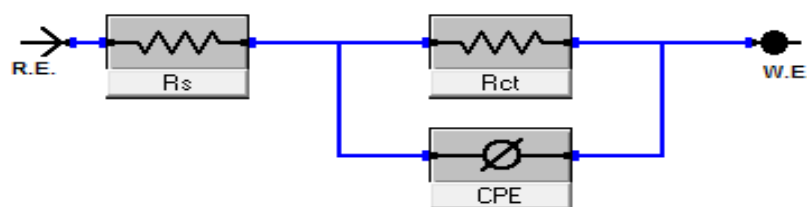


**Figure 3:** Equivalent circuit used to model impedance data in 1 M HNO<sub>3</sub> solutions

The semi-circle diameter represented the charge transfer resistance,  $R_{ct}$ , equivalent to the polarization resistance,  $R_p$ , and inversely proportional to the  $i_{corr}$  value. An increase in  $R_{ct}$  referred to an increase in the thickness of the

double layer that adsorbed by inhibitor [18]. In addition, the values of the double-layer capacitance ( $C_{dl}$ ) decreased by adding inhibitor into corrosive solution. Additionally, double layer capacitance could be calculated with the following equation:

$$C_{dl} = \epsilon \epsilon_0 (A/\delta) \tag{5}$$

where  $\epsilon$  was the double-layer dielectric constant,  $\epsilon_0$  the vacuum electrical permittivity,  $\delta$  the double-layer thickness, and  $A$  was the surface area. Mainly, the decrease in  $C_{dl}$  value was attributed to the replacement of the adsorbed water molecules at the metal surface by the inhibitor molecules having lower dielectric constant [19]. Also, the decrease in surface area which acted as a site for charging may be considered as another reason for the  $C_{dl}$  decrease [19]. These points suggested that the role of inhibitor molecules was preceded by its adsorption at the metal–solution interface.

**Table 4:** Electrochemical kinetic parameters obtained from EIS technique for copper in 1M HNO<sub>3</sub> in the absence and presence of different concentrations of investigated compounds at 25°C

Comp	Conc., x 10 <sup>6</sup> M	R <sub>s</sub> , Ω cm <sup>2</sup>	Y <sup>o</sup> , μΩ <sup>-1</sup> s <sup>n</sup> cm <sup>-2</sup>	n	R <sub>ct</sub> , Ω cm <sup>2</sup>	C <sub>dl</sub> , μFcm <sup>-2</sup>	θ	%IE
Blank	0.0	1.454	464.9	0.665	187	135.97	---	---
A	5	1.703	184.1	0.716	1113	98.17	0.831	83.1
	10	1.665	119.2	0.749	1633	68.88	0.885	88.5
	15	1.847	65.8	0.779	2117	37.71	0.911	91.1
	20	1.819	24.3	0.881	2503	16.06	0.925	92.5
	25	1.924	18.9	0.851	3299	13.08	0.940	94.0
	30	1.968	13.0	0.80	3692	11.59	0.949	94.9
B	5	1.733	207.0	0.761	559	101.37	0.665	66.5
	10	1.788	159.0	0.717	785	74.33	0.761	76.1
	15	1.745	141.6	0.744	1013	62.64	0.815	81.5
	20	1.618	133.5	0.716	1231	52.13	0.848	84.8
	25	1.743	118.6	0.702	1399	43.38	0.866	86.6
	30	1.906	59.81	0.803	1908	35.14	0.901	90.1
C	5	1.885	261.5	0.777	350	116.52	0.466	46.6
	10	1.996	243.0	0.731	362	99.37	0.484	48.4
	15	2.012	198.2	0.728	443	95.73	0.577	57.7
	20	1.831	148.8	0.747	491	90.23	0.619	61.9
	25	1.865	131.5	0.781	587	64.18	0.681	68.1
	30	1.706	107.7	0.732	869	59.35	0.784	78.4
D	5	1.909	424	0.670	228	127.94	0.179	17.9
	10	1.882	284	0.724	302	117.87	0.382	38.2
	15	1.957	274	0.711	398	109.44	0.530	53.0
	20	1.806	253	0.706	467	110.1	0.601	60.1
	25	1.745	251	0.706	500	106.60	0.626	62.6
	30	1.807	244	0.665	783	103.87	0.761	76.1

The electrochemical parameters were listed in Table 4. The inhibition efficiency was calculated from the charge transfer resistance data from Eq (2). The order of inhibition efficiency obtained from EIS measurements is as follows:

$$A > B > C > D$$

### 3.3. Electrochemical Frequency Modulation (EFM) Technique

EFM is a nondestructive corrosion measurement technique that can directly and quickly determine the corrosion current values without prior knowledge of Tafel slopes, and with only a small polarizing signal. These advantages

of EFM technique make it an ideal candidate for online corrosion monitoring [20]. The great strength of the EFM is the causality factors which serve as an internal check on the validity of EFM measurement. The causality factors CF-2 and CF-3 were calculated from the frequency spectrum of the current responses.

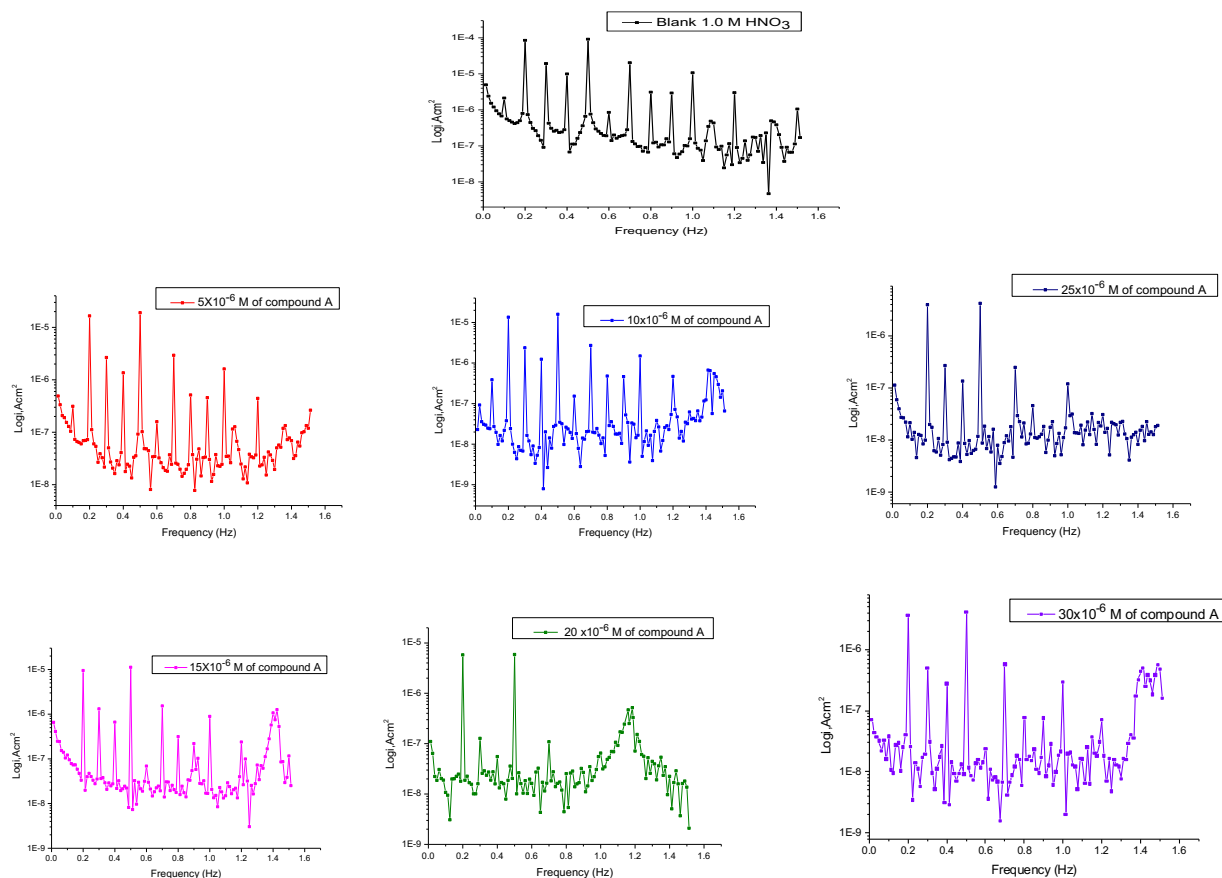


**Figure 4:** EFM spectra for copper in 1M HNO<sub>3</sub> in the absence and presence of different concentrations of compound (A) at 25°C.

Figure 4 has shown the EFM intermodulation spectra (current vs. frequency) of copper in nitric acid solution containing different concentrations of compound (A). Similar intermodulation spectra were obtained for other compounds (not shown). Each spectrum was a current response as a function of frequency. The larger peaks were used to calculate the corrosion current density ( $i_{corr}$ ), the Tafel slopes ( $\beta_c$  and  $\beta_a$ ) and the causality factors (CF-2 and CF-3). These electrochemical parameters were listed in Table 5. The data presented in Table 5 obviously showed that, the addition of any one of tested compounds at a given concentration to the acidic solution decreased the corrosion current density, indicating that these compounds have inhibited the corrosion of copper in 1 M HNO<sub>3</sub> through adsorption.

The causality factors obtained under different experimental conditions were approximately equal to the theoretical values (2 and 3) indicating that the measured data were verified and of good quality [12]. The inhibition efficiencies %IE<sub>EFM</sub> increase by increasing the inhibitor concentrations and was calculated from equation (6):

$$\%IE_{EFM} = \theta_{coverage} \times 100 = [1 - (i_{corr}/i_{corr}^0)] \times 100 \quad (6)$$

where  $i_{corr}^0$  and  $i_{corr}$  were corrosion current densities in the absence and presence of inhibitor, respectively.

The inhibition sufficiency obtained from this method was in the order:

$$A > B > C > D$$



**Table 5:** Electrochemical kinetic parameters obtained by EFM technique for copper corrosion in the absence and presence of various concentrations of inhibitors in 1M HNO<sub>3</sub> at 25°C

Comp	Conc., x 10 <sup>6</sup> M	i <sub>corr</sub> , μA cm <sup>-2</sup>	β <sub>c</sub> , mVdec <sup>-1</sup>	β <sub>a</sub> , mVdec <sup>-1</sup>	CF-2	CF-3	C.R, mpy	θ	%IE
Blank	0.0	138.1	154.3	59.9	1.93	2.94	133.1	---	---
A	5	25.6	172.9	64.7	1.89	3.20	24.68	0.814	81.4
	10	18.70	147.9	57.6	1.86	2.51	18.03	0.864	86.4
	15	15.15	160.2	68.1	1.83	2.42	14.60	0.889	88.9
	20	13.8	170.0	90.3	1.96	2.25	13.25	0.902	90.2
	25	9.70	190.4	88.5	2.10	2.31	9.29	0.929	92.9
	30	6.98	210.3	98.4	1.87	2.57	6.73	0.949	94.9
B	5	27.81	108.3	56.6	1.88	3.30	26.74	0.798	79.8
	10	26.82	149.5	57.1	1.87	1.95	25.87	0.806	80.6
	15	18.74	171.8	70.2	1.83	2.17	18.06	0.864	86.4
	20	16.20	155.2	62.4	1.86	2.35	15.61	0.890	89.0
	25	14.21	177.1	56.7	1.85	2.59	13.63	0.897	89.7
	30	11.68	147.8	94.4	2.11	2.99	11.26	0.913	91.3
C	5	45.38	125.8	52.2	1.93	3.25	43.74	0.666	67.1
	10	40.61	136.9	54.3	1.89	3.19	39.14	0.695	70.5
	15	37.16	109.7	51.5	1.91	2.82	35.16	0.730	73.0
	20	28.43	114.4	27.4	1.90	3.28	27.41	0.782	79.2
	25	26.15	186.2	53.3	1.86	3.17	25.21	0.811	81.0
	30	25.61	172.9	64.7	1.88	3.10	24.68	0.826	81.4
D	5	108.6	138.4	56.7	1.91	3.21	104.7	0.217	21.7
	10	59.12	161.7	54.2	1.88	2.83	56.98	0.565	57.1
	15	47.34	160.2	55.5	1.86	3.16	45.63	0.659	65.9
	20	40.19	151.3	58.4	1.91	3.17	38.73	0.710	71.0
	25	35.72	165.1	55.1	2.11	2.74	33.28	0.741	74.1
	30	29.43	170.9	57.0	1.90	3.24	28.37	0.789	78.6

### 3.4. Weight loss measurements

The weight losses of copper specimen in 1 M HNO<sub>3</sub> solution, with and without different concentrations of the investigated derivatives, were determined after 6 hours of immersion at 25°C. Figure 5 represents this for compound (A) as an example. Similar curves were obtained for other compounds (not shown). Obtained values of %IE are given in Table 6 at different concentrations from the investigated compounds. The results obtained have shown that the addition of investigated compounds has decreased the weight loss (mg cm<sup>-2</sup>) and the corrosion rate (mg cm<sup>-2</sup> min<sup>-1</sup>). The inhibition efficiency (%IE) and the degree of surface coverage, θ, of 4-hydroxycoumarin derivatives for the corrosion of copper was calculated from Eq (1). The inhibition achieved by these compounds decreases in the following order:

$$(A) > (B) > (C) > (D)$$

The observed inhibition action of the 4-hydroxycoumarin derivatives could be attributed to the adsorption of their components on copper surface. The formed layer of the adsorbed molecules must have isolated the metal surface from the aggressive medium which limited the dissolution of the latter by blocking of their corrosion sites and hence decreasing the corrosion rate, with increasing efficiency as their concentrations were increase [21].

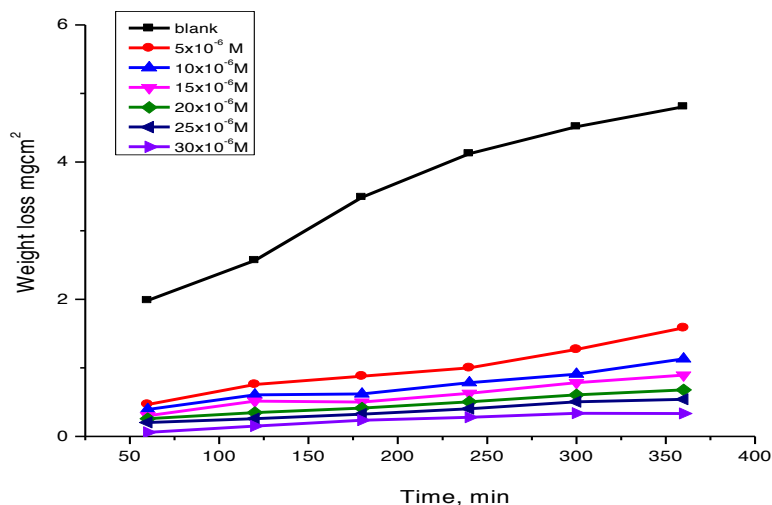


**Figure 5:** Weight loss-time curves for the corrosion of copper in absence and presence of different concentrations of compound (A) at 25°C

**Table 6:** Inhibition efficiency of different concentrations of investigated compounds at 180 min for copper corrosion in 1M HNO<sub>3</sub> solution as determined from weight loss method at 25°C

Comp.	A		B		C		D	
	$\Theta$	% IE	$\Theta$	% IE	$\Theta$	% IE	$\Theta$	% IE
0.0	---	---	---	---	---	---	---	---
5	0.759	75.9	0.598	59.8	0.502	50.2	0.414	41.4
10	0.822	82.2	0.642	64.2	0.563	56.3	0.525	52.5
15	0.856	85.6	0.689	68.9	0.609	60.9	0.545	54.5
20	0.881	88.1	0.726	72.6	0.657	65.7	0.620	62.0
25	0.907	90.7	0.755	75.5	0.702	70.2	0.642	64.2
30	0.923	92.3	0.774	77.4	0.736	73.6	0.683	68.3

### 3.5. Effect of Temperature

The effect of temperature on the inhibited acid-metal reaction is highly complex, because many changes occur on the metal surface, such as rapid etching and desorption of the inhibitor and the inhibitor itself, in some cases, may undergo decomposition or rearrangement, and the corrosion rate increases with the rise of temperature. The effect of temperature on the corrosion rate of copper in 1M HNO<sub>3</sub> and in the presence of different inhibitor concentrations was studied in the temperature range of 298–318K using weight loss measurements. It was found that the inhibition efficiency decreased with increasing temperature but at lower rate than in uninhibited solutions with increasing the concentration of the inhibitor, as shown in Table 7. From the data of Table 8 for compound (A) illustrated that the adsorption was decreased with increasing the temperature and corrosion rate (C.R.). Similar Tables were obtained for the other compounds (not shown). It has shown that the raise in temperature led to the reduction of the inhibitor adsorption and then the acceleration of dissolution process. i.e. the adsorption behavior of inhibitors on copper surface in 1M HNO<sub>3</sub> occurs through physical adsorption. The increase of % IE with increase in the temperature has shown the change in the nature of the adsorption mode; the inhibitor was being physically adsorbed at lower temperatures, while chemisorption was favored when the temperature was increased.

**Table 7:** Inhibition efficiency (%IE) of 4-hydroxycoumarin derivatives at different concentrations of the inhibitors for copper corrosion after 180 min in 1M HNO<sub>3</sub> solution at different temperatures from weight-loss measurements

Conc., x10 <sup>6</sup> M	% IE															
	Compound (A)				Compound (B)				Compound (C)				Compound (D)			
	303 K	308 K	313 K	318 K	303 K	308 K	313 K	318 K	303 K	308 K	313 K	318 K	303 K	308 K	313 K	318 K
5	63.7	61.5	54.4	41.0	46.8	39.8	36.7	30.2	41.2	37.4	34.9	27.7	31.5	28.3	26.4	23.5
10	71.5	67.9	61.9	48.9	55.9	48.5	43.6	36.8	51.3	47.7	41.9	33.5	37.5	35.1	33.8	30.5
15	75.4	71.9	66.4	52.6	59.2	52.4	48.0	40.9	55.8	52.0	45.7	36.9	43.1	40.3	37.8	35.4
20	77.5	76.3	70.7	56.2	62.4	57.1	51.8	43.7	60.5	55.9	50.9	41.0	48.6	44.2	41.7	38.0
25	79.7	78.1	72.8	60.3	66.1	60.6	54.6	46.4	64.7	59.0	55.7	44.2	51.0	48.3	45.0	41.7
30	82.1	80.4	75.5	63.4	69.4	63.9	60.5	49.6	66.4	62.7	59.8	46.7	54.6	52.4	48.7	44.8

**Table 8:** Values of inhibition efficiencies %IE, surface coverage (Θ) and corrosion rate (C.R.) from weight-loss measurements for copper corrosion after 180 min immersion in 1M HNO<sub>3</sub> in the absence and presence of different concentrations of compound (A) at different temperatures

Conc., x 10 <sup>6</sup> M		298 K	303 K	308 K	313 K	318 K
0	C.R.x10 <sup>-3</sup>	19.3	22.8	35.0	45.6	57.9
5	Θ	0.759	0.637	0.615	0.544	0.410
	% IE	75.9	63.7	61.5	54.4	41.0
	C.R.x10 <sup>-3</sup>	4.9	7.5	13.5	20.7	34.1
10	Θ	0.822	0.715	0.679	0.619	0.489
	% IE	82.2	71.5	67.9	61.9	48.9
	C.R.x10 <sup>-3</sup>	3.4	6.5	11.5	17.3	29.8
15	Θ	0.856	0.754	0.719	0.664	0.526
	% IE	85.6	75.4	71.9	66.4	52.6
	C.R.x10 <sup>-3</sup>	2.8	5.6	9.8	15.3	27.4
20	Θ	0.881	0.775	0.763	0.707	0.562
	% IE	88.1	77.5	76.3	70.7	56.2
	C.R.x10 <sup>-3</sup>	2.3	4.6	8.3	13.8	25.3
25	Θ	0.907	0.797	0.781	0.728	0.603
	% IE	90.7	79.7	78.1	72.8	60.3
	C.R.x10 <sup>-3</sup>	1.8	4.1	7.1	12.1	22.7
30	Θ	0.923	0.821	0.804	0.755	0.634
	% IE	92.3	82.1	80.4	75.5	63.4
	C.R.x10 <sup>-3</sup>	1.4	3.3	6.3	11.0	21.1

In Figure 6, variation of inhibition efficiency of compound (A) is shown at different temperatures using various concentrations of compound (A) for copper corrosion in 1M HNO<sub>3</sub> (similar curves were obtained in presence of the other compounds, but not shown).

### 3.6. Kinetic –thermodynamic corrosion parameters

The activation energy (E<sub>a</sub><sup>\*</sup>) of the corrosion process was calculated using Arrhenius equation (6) [22]:

$$k = A \exp(-E_a^* / RT) \quad (6)$$

where k is corrosion rate, A was Arrhenius constant, E<sub>a</sub><sup>\*</sup> the values of activation energies, R was the gas constant and T was the absolute temperature. The values of activation energies E<sub>a</sub><sup>\*</sup> could be obtained from the slope of the

straight lines of plotting  $\log k$  vs.  $1/T$  in the presence and absence of investigated compounds at various temperatures, and are given in Table 9. Figure 7 shows the linear regression. ( $R^2$ ) was close to 1 which indicated that the corrosion of copper in 1 M  $\text{HNO}_3$  solution could be elucidated using the kinetic model in Table 9.

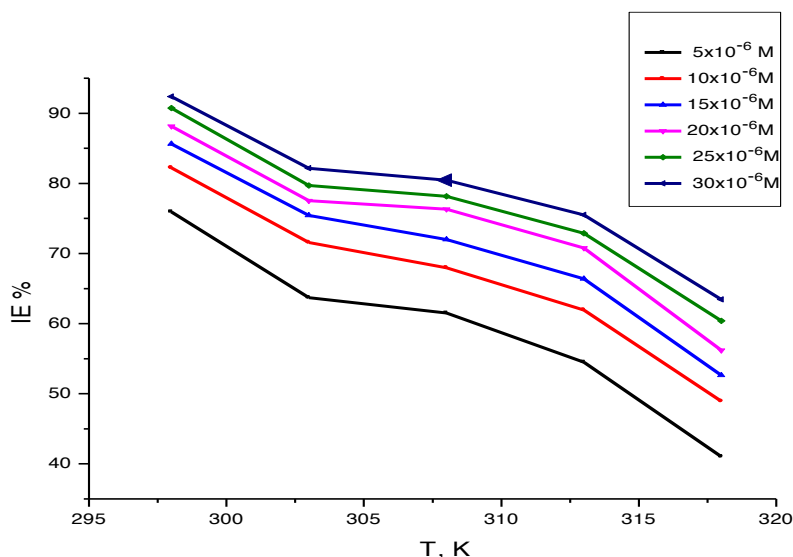


**Figure 6:** Effect of temperature on % IE at various concentrations of compound (A) for copper corrosion in 1M  $\text{HNO}_3$  with different temperatures

The effective activation energies have shown higher values in the presence of these compounds than in the absence of them. Therefore, the inhibitor retarded the corrosion process at lower temperature but this inhibition action was reduced at higher temperature. The calculated effective activation energies have shown that the investigated compounds have inhibited corrosion more effectively at higher concentrations. Also, increase in activation energies with the addition of gradually increasing concentrations of investigated compounds has indicated that the energy barrier for the corrosion reaction has increased. These values have indicated that the presence of these inhibitors has increased the activation energy of the metal dissolution reaction and that the process was diffusion controlled ( $E_a^* > 40 \text{ kJ mol}^{-1}$ ). The activation in the blocking of the active sites must be associated with an increase in the activation energy of copper corrosion in the inhibited state [23]. The activation energy for the corrosion of copper in 1 M  $\text{HNO}_3$  was found to be  $32 \text{ kJ mol}^{-1}$  which is in good agreement with the work carried out by Fouda et al [24] and others [25]. Enthalpy and entropy of activation ( $\Delta H^*$ ,  $\Delta S^*$ ) were calculated from transition state theory using the equation (7) [25]:

$$k = RT/Nh \exp(\Delta S^*/R) \exp(-\Delta H^*/RT) \quad (7)$$

where  $h$  is Planck's constant,  $N$  is Avogadro's number,  $\Delta S^*$  is the entropy of activation and  $\Delta H^*$  is the enthalpy of activation. Figure 8 shows a plot of  $\log(k/T)$  vs.  $(1/T)$ . The straight lines were obtained with a slope of  $(\Delta H^*/2.303 R)$  and an intercept of  $(\log R/Nh + \Delta S^*/2.303 R)$  and with linear regression ( $R^2$ ) was close to 1 from which the values of  $\Delta H^*$  and  $\Delta S^*$  were calculated and also listed in Table 9.

From inspection of Table 9, it was clear that the positive values of  $\Delta H^*$  reflected the process of adsorption of the inhibitors on the copper surface was an endothermic process; it was attributable unequivocally to chemisorption [26]. Typically, the enthalpy of a chemisorption process approached  $(100 \text{ kJ mol}^{-1})$  [27]. From these results, it was clear that the values of  $\Delta H^*$  reflected strong adsorption of these compounds on the copper surface. Moreover, the increase in the activation enthalpy ( $\Delta H^*$ ) in presence of the inhibitors meant that the addition of 4-Hydroxycoumarin derivatives to 1 M  $\text{HNO}_3$  solution increased the height of the energy barrier of the corrosion reaction to an extent depending on the concentration of the present compounds. The adsorption of investigated compounds on the metal surface lead to a lower number of hydrogen atoms adsorbed on it; this caused a decrease

in hydrogen evolution rate rather than the rate of metal dissolution, because of the blocking of the surface of the metal by adsorbed molecules of the inhibitor. The values of  $\Delta S^*$  in the absence and presence of these investigated compounds were large and negative; this indicated that the activated complex in the rate-determining step represented an association rather than dissociation step, so that a decrease in disordering took place on going from reactants to the activated complex and the activated molecules were in higher order state than that at the initial state [28].

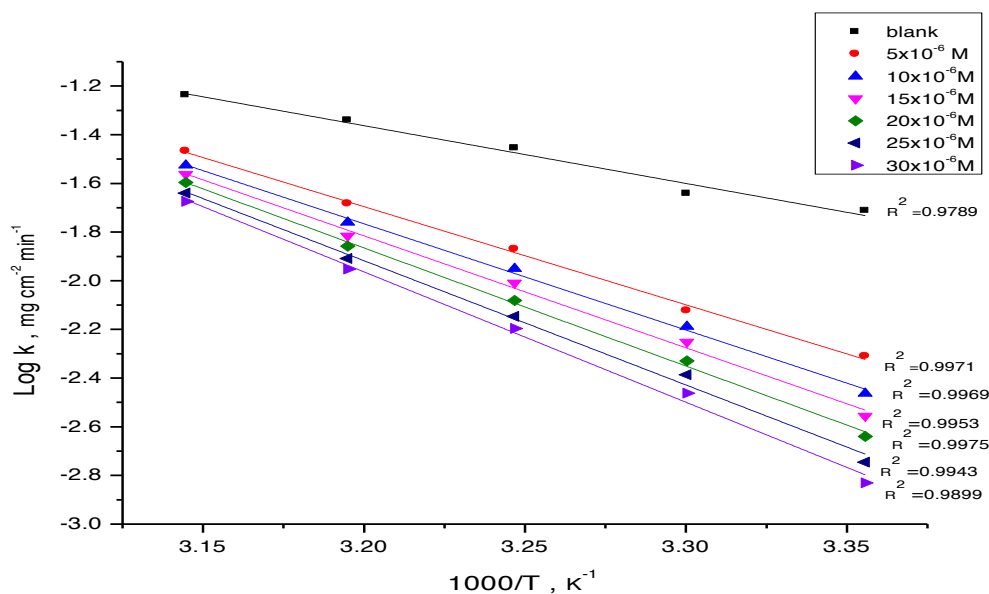


**Figure 7:** Arrhenius plots of variation of  $\log k$  (corrosion rate) vs.  $1/T$  for the dissolution of copper in 1M  $\text{HNO}_3$  in the absence and presence of different concentrations of compound (A)

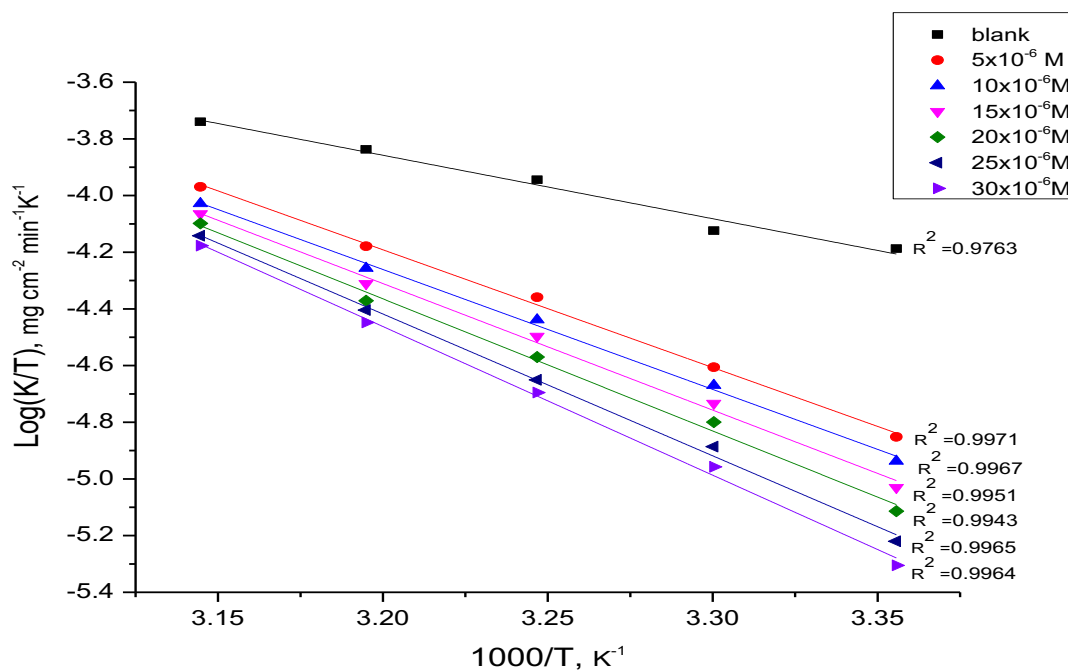


**Figure 8:** Plots of  $(\log k / T)$  vs.  $1/T$  for the dissolution of copper in 1M  $\text{HNO}_3$  in the absence and presence of different concentrations of compound (A)

**Table 9:** Kinetic activation parameters for copper in 1M HNO<sub>3</sub> in the absence and presence of different concentrations of investigated inhibitors

Comp	Conc., x 10 <sup>6</sup> M	E <sub>a</sub> <sup>*</sup> , kJ mol <sup>-1</sup>	ΔH <sup>*</sup> , kJ mol <sup>-1</sup>	-ΔS <sup>*</sup> , J mol <sup>-1</sup> K <sup>-1</sup>
Blank	0.0	45.5	43.1	134
A	5	77.2	74.6	63.5
	10	83.5	81.0	45.9
	15	88.0	85.5	28.6
	20	92.6	89.3	16.4
	25	97.7	95.8	11.3
	30	92.5	100.4	4.3
B	5	57.6	56.9	92.3
	10	62.9	59.5	85.7
	15	69.6	67.2	62.4
	20	72.0	69.5	54.9
	25	74.0	71.6	49.4
	30	75.2	73.1	47.0
C	5	54.0	56.3	94.5
	10	60.1	57.6	91.1
	15	62.2	60.0	84.0
	20	63.1	61.4	81.3
	25	66.0	64.0	73.0
	30	71.0	68.6	59.3
D	5	52.1	52.4	106.2
	10	58.0	55.5	97.2
	15	59.0	58.4	88.4
	20	60.5	60.2	79.5
	25	62.3	63.0	74.9
	30	64.6	66.1	65.4

### 3.7. Adsorption isotherms

One of the most convenient ways of expressing adsorption quantitatively is by deriving the adsorption isotherm that characterizes the metal/inhibitor/ environment system [29]. The basic information on the interaction between the inhibitor and the metal surface can be provided by the adsorption isotherm, and the type of the inhibitors on metal is influenced by (i) the nature and charge of the metal (ii) chemical structure of the inhibitor and (iii) the type of electrolyte [30]. Attempts were made to fit (θ) values to various adsorption isotherms. The Temkin adsorption isotherm [31].fitted well to the experimental data

$$\Theta = (2.303/a) \text{Log } K_{\text{ads}} + (2.303/a) \log C \quad (8)$$

Where θ is the degree of surface coverage (θ = % IE/100), K<sub>ads</sub> is the adsorption equilibrium constant, C is the concentration (mol L<sup>-1</sup>) of the inhibitor and “a” (heterogeneous factor of metal surface) is a molecular interaction parameter depending upon molecular interactions. A plot of θ versus log C should give the straight lines with slopes equal to (2.303/a) and the intercept is (2.303/a) logK<sub>ads</sub>. In order to get a comparative view, the variation of the adsorption equilibrium constant (K<sub>ads</sub>) of the inhibitors with their molar concentrations was calculated according to Eq (8). The experimental data provided good curves fitting for the applied adsorption isotherm as the correlation coefficients (R<sup>2</sup>) close to unity which were in the range (0.979-0.998). The values obtained of “a”, “1/y”, K<sub>ads</sub> and ΔG<sup>o</sup><sub>ads</sub> are given in Table 10. The equilibrium constant (K<sub>ads</sub>) of adsorption process was determined using Eq. (9) which could be further used to determine free energy of adsorption (ΔG<sup>o</sup><sub>ads</sub>) as follows:

$$\Delta G^{\circ}_{\text{ads}} = -RT \ln (55.5 K_{\text{ads}}) \quad (9)$$

where 55.5 is the molar concentration of water in the solution in mol L<sup>-1</sup>, T is the absolute temperature and R is the universal gas constant.

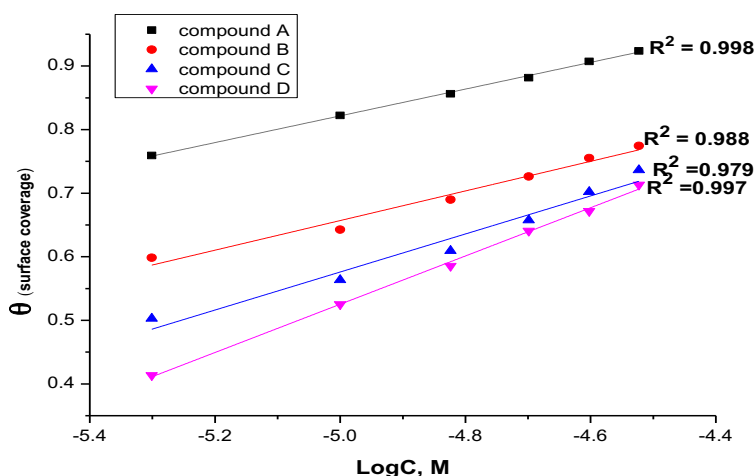


**Figure 9:** Curve fitting of corrosion data for copper in 1M HNO<sub>3</sub> in presence of different concentrations of investigated compounds to the Temkin adsorption isotherm at 25°C

It is clear that the adsorption of inhibitors on the copper surface follow Temkin isotherm. Figure 9 represents the plot of  $\theta$  against  $\log C$  for investigated compounds. As can be seen from this Figure, the Temkin isotherm was the best one which explained the experimental results. These results confirmed the assumption that, these compounds were adsorbed on the metal surface through the lone pair of electrons of hetero atoms. In addition, the extent of inhibition was directly related to the performance of adsorption layer which was a sensitive function of the molecular structure. The  $\Delta G^{\circ}_{ads}$  and  $K_{ads}$  values for investigated compounds were calculated and are recorded in Table 11. Besides, it was found that the kinetic-thermodynamic model of El-Awady et al [32] is valid to operate the present adsorption data equation (11):

$$\text{Log}(\theta / (1-\theta)) = \text{Log } K' + y \text{ Log } C \quad (11)$$

where  $C$  is concentration of the inhibitor and the equilibrium constant of adsorption  $K_{ads} = K' (1/y)$ , where  $1/y$  is the number of the surface active sites occupied by one inhibitors molecule. The calculated values of  $1/y$ , "a",  $K_{ads}$  and  $\Delta G^{\circ}_{ads}$  are in general, the values of  $\Delta G^{\circ}_{ads}$  were obtained from El-Awady et al model were comparable with those obtained from Temkin's isotherm at 25°C are given in Table 11. Figure 10 represents the plot of  $\text{Log}(\theta / (1-\theta))$  against  $\log C$  for compounds (A) at different temperatures as an example. Similar curves were obtained for other compounds (not shown). Table 12 shows the effect of temperature on adsorption for compound (A).

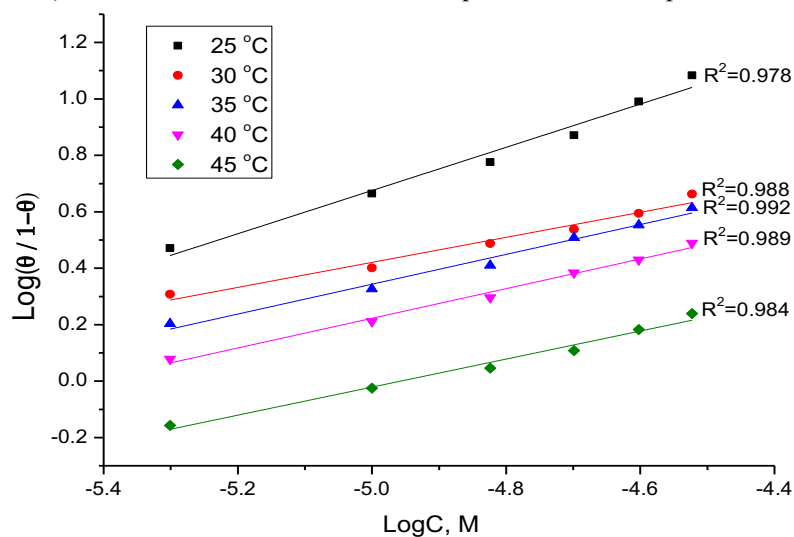


**Figure 10:** Adsorption isotherm curves from kinetic-thermodynamic model for the adsorption of compound (A) on copper in 1M HNO<sub>3</sub> at various temperatures

**Table 10:** Some parameters from kinetic-thermodynamic model of El-Awady et al model for copper in 1M HNO<sub>3</sub> for compound (A) at different temperatures

Compound	Temp., K	1/y	K <sub>ads</sub> , x 10 <sup>-5</sup> , M <sup>-1</sup>	-ΔG <sup>o</sup> <sub>ads</sub> , kJ mol <sup>-1</sup>
A	298	1.31	2.11	44.2
	303	2.25	1.95	44.0
	308	1.89	1.91	44.3
	313	1.90	1.85	43.9
	318	2.01	1.80	43.8

The values of ΔG<sup>o</sup><sub>ads</sub> around 44 kJ mol<sup>-1</sup> indicated that this compound (A) was mixed adsorbed (chemisorption and physisorption) on copper surface at all the temperature ranges studied but the adsorption and inhibition efficiency decreased with an increase in temperature

**Table 11:** Some parameters from Temkin isotherm and the kinetic-thermodynamic model of El-Awady et al for copper in 1M HNO<sub>3</sub>for investigated compounds 25°C

Comp	Temkin			Kinetic model		
	a	K <sub>ads</sub> , M <sup>-1</sup> x10 <sup>-7</sup>	-ΔG <sup>o</sup> <sub>ads</sub> kJ mol <sup>-1</sup>	1/y	K <sub>ads</sub> , M <sup>-1</sup> x10 <sup>-5</sup>	-ΔG <sup>o</sup> <sub>ads</sub> kJ mol <sup>-1</sup>
A	10.95	7.744	45.1	1.31	1.99	44.2
B	9.88	3.944	43.2	2.13	1.74	39.9
C	7.68	1.396	41.7	1.78	1.28	39.0
D	6.67	0.909	40.1	1.45	1.00	38.4

From these results, it could be generalized that more efficient inhibitor has more negative ΔG<sup>o</sup><sub>ads</sub> value so that from the tabulated values of ΔG<sup>o</sup><sub>ads</sub> the order of inhibition efficiency was as follows: A > B > C > D. Generally, values of ΔG<sup>o</sup><sub>ads</sub> around -20 kJ mol<sup>-1</sup> or lower are consistent with the electrostatic interaction between the charged molecules and the charged metal physisorption. The calculated ΔG<sup>o</sup><sub>ads</sub> values were higher than -40 kJ mol<sup>-1</sup> indicating that the adsorption mechanism of the inhibitors on copper corrosion in 1M HNO<sub>3</sub> solutions was typical chemisorption. The unshared electron pairs in, nitrogen and oxygen might have interacted with copper atoms. Moreover, the values of "a" were positive in all cases showing that attraction in the adsorption layer [33]. It is worth noting that the value of (1/y) was more than unity. This meant that the given inhibitor molecules must have occupy more than one active site. The values of K<sub>ads</sub> were found to run parallel to the % IE (K<sub>A</sub>> K<sub>B</sub>> K<sub>C</sub>> K<sub>D</sub>). This result reflected the increasing capability, due to structural formation, on the metal surface [34]. Also thermodynamic parameters, heat of adsorption (ΔH<sup>o</sup><sub>ads</sub>) and the standard entropy (ΔS<sup>o</sup><sub>ads</sub>) can be determined by Plot of (ΔG<sup>o</sup><sub>ads</sub>) versus T in Figure11 according to the thermodynamic basic equation (12). The experimental data have given good curves fitting as the correlation coefficients (R<sup>2</sup>) was close to unity with the range (0.992-0.999):

$$\Delta G^{\circ}_{ads} = \Delta H^{\circ}_{ads} - T \Delta S^{\circ}_{ads} \quad (12)$$

The values of thermodynamic parameters for the adsorption of inhibitors from Temkin isotherm were calculated at temperature (25°C- 45°C) and are recorded in Table 12, which can provide valuable information about the mechanism of corrosion inhibition. While an endothermic adsorption process (ΔH<sup>o</sup><sub>ads</sub> > 0) is attributed unequivocally to chemisorption [35], an exothermic adsorption process (ΔH<sup>o</sup><sub>ads</sub> < 0) may involve either physisorption or chemisorption or mixture of both the processes. The absolute values of ΔH<sup>o</sup><sub>ads</sub> obtained in this study was lower than (100 kJ mol<sup>-1</sup>) which is indicative of physisorption [36].



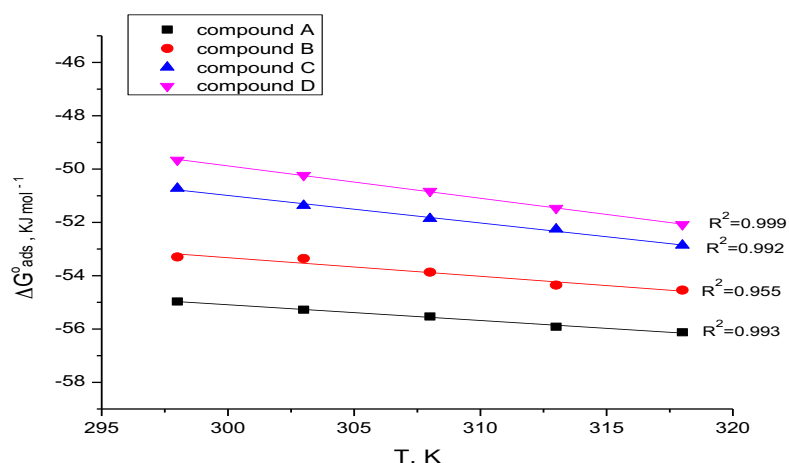


**Figure 11:** Plots of  $\Delta G_{\text{ads}}^{\circ}$  vs. T for the adsorption of investigated inhibitors on copper in 1M  $\text{HNO}_3$

The above calculated values show that the values of  $\Delta G_{\text{ads}}^{\circ}$  are around 45-35  $\text{kJ mol}^{-1}$  and the absolute values of  $\Delta H_{\text{ads}}^{\circ}$  obtained in this study was lower than 40  $\text{kJ mol}^{-1}$  which have indicated that the adsorption mechanism of investigated compounds on copper in 1M  $\text{HNO}_3$  solution at the studied temperatures was mix of physisorption and chemisorptions. The entropy of adsorption obtained was large and positive because inhibitor molecule were freely moving in the bulk solution, and were adsorbed in an orderly fashion onto the copper, resulting into a decrease in entropy [37]. From thermodynamic principles, since the adsorption was an exothermic process, it must be accompanied by a decrease in entropy [38]. Also, this confirmed from the decrease of % IE with increase in temperature and the higher values of  $E_a^*$  (activation energies) obtained in the presence of inhibitor compared with its absence. The higher values of  $K_{\text{ads}}$  for investigated inhibitors have indicated stronger adsorption on the copper surface in 1M  $\text{HNO}_3$  solution. The strong interaction of inhibitor with copper surface could be attributed to the presence of N, O atoms and  $\pi$ -electrons in the inhibitor molecules.

**Table 12:** Thermodynamic parameters from Temkin isotherm model for copper in 1 M  $\text{HNO}_3$  for investigated compounds at different temperatures

Comp	Temp., K	$K_{\text{ads}} \times 10^{-7}, \text{M}^{-1}$	a	$-\Delta G_{\text{ads}}^{\circ}, \text{kJ mol}^{-1}$	$-\Delta H_{\text{ads}}^{\circ}, \text{kJ mol}^{-1}$	$\Delta S_{\text{ads}}^{\circ}, \text{J mol}^{-1} \text{K}^{-1}$	$R^2$
A	298	7.744	10.95	45.1	37.5	58.5	0.999
	303	6.067	10.03	45.0			0.998
	308	4.698	9.47	44.5			0.997
	313	3.845	8.51	44.0			0.999
	318	2.971	8.21	43.1			0.998
B	298	3.944	9.88	43.2	32.2	70.1	0.991
	303	2.831	8.30	53.3			0.995
	308	2.460	7.98	43.0			0.998
	313	2.113	8.02	42.3			0.997
	318	1.633	7.85	41.5			0.998
C	298	1.396	7.68	41.7	20.1	103.2	0.997
	303	1.297	7.52	40.3			0.996
	308	1.127	7.34	39.8			0.997
	313	0.944	7.45	38.2			0.996
	318	0.865	7.72	36.8			0.998
D	298	0.909	6.67	40.1	12.6	123.8	0.988
	303	0.818	7.62	37.9			0.999
	308	0.748	7.87	35.8			0.997
	313	0.696	8.30	34.4			0.988
	318	0.643	7.94	30.0			0.996

### 3.8. Surface morphology analysis

The formation of a protective surface film of inhibitor at the electrode surface was further confirmed by scanning electron microscopy (SEM) of the metal surface. Also, in order to see whether the 4-Hydroxycoumarin molecules are adsorbed on the copper surface or not, energy dispersive X-ray (EDX) experiments were also carried out. Figure 12 shows the SEM micrograph of fresh pure copper surface with and without any additions of acid or the inhibitor. There was a marked improvement in the surface morphology of copper that was treated with the inhibitor (the rate of corrosion is suppressed) due to the formation of an adsorbed protective film of the inhibitor at the test sample surface. The corresponding EDX profile analysis is presented in Figure 13. The EDX survey spectra were used to determine which elements of inhibitor were present on the electrode surface before and after exposure to the inhibitor solution. For the specimen without inhibitor treatment only copper was detected. This was confirmed by using EDX. The main corrosion products formed on exposed copper to nitric acid were identified as the basic copper nitrate, gerhardtite ( $\text{Cu}_2(\text{NO}_3)(\text{OH})_3$ ) and to a smaller extent cuprite ( $\text{Cu}_2\text{O}$ ) [39]. It was noticed that there was existence of the carbon and oxygen peak in the EDX spectra in the case of the sample exposed to the inhibitor which could be attributed to the adsorption of organic moiety at the copper surface. The increase in amount of carbon atom in the case of the order  $A > B > C > D$  as shown in Tables 13, has indicated that the dissolution of copper is very much inhibited by compound (A) and compound (B) thereby showing a very highly protective capacity and a strong enrichment with carbon as noted in the case of compound (A and B), which is shown in Table 13, in contrast to the protective films formed by the compound (C) and compound (D). The spectra of Figure 13 show that the oxygen signals are considerably suppressed relative to the samples prepared in 1M  $\text{HNO}_3$  solution, and certainly this suppression would increase with increasing investigated compounds concentrations and immersion time. The suppression of the oxygen signals has taken place because of the overlying inhibitor film. Also it is important to notice the extent of covered surface of copper by adsorbed layer of inhibitors. The peaks of EDX spectra increased in the presence of inhibitor especially in the case of compound (A) in a comparison of EDX analysis obtained in the absence of inhibitor. Also it may be indicating that the investigated derivatives molecules protecting the copper surface against acid corrosion according to the order of:  $A > B > C > D$ . But the surface of the metal may not be covered completely by the investigated molecules due to the short immersion time. The composition of the detected elements on the copper surface indicated that the inhibitor molecules were strongly adsorbed on the copper forming a Cu-investigated molecule bond, thus preventing the surface against corrosion.

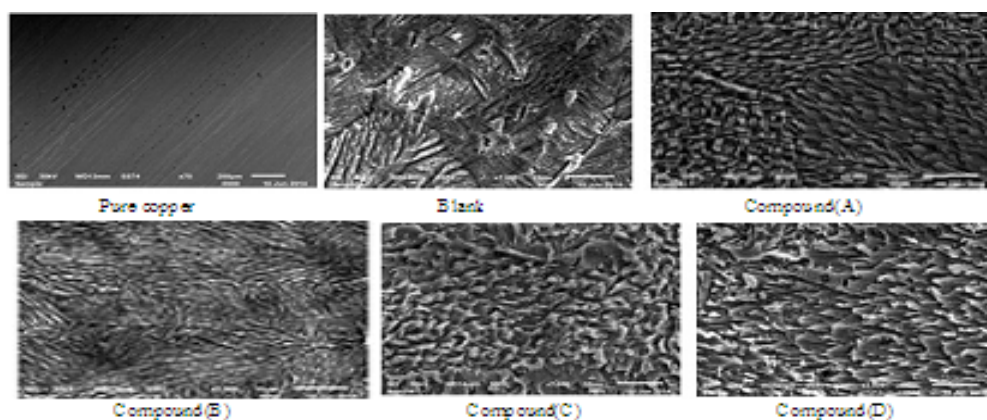


**Figure 12:** SEM micrographs for copper in the absence and presence of  $30 \times 10^{-6}$  M after 6 hours immersion of investigated compounds (A-D) at  $25^\circ\text{C}$

### 3.9. Chemical Structure and Corrosion Inhibition

Inhibition of the corrosion of copper in 1 M  $\text{HNO}_3$  solutions by some 4-hydroxycoumarin derivatives, determined by potentiodynamic polarization measurements, was found to depend on concentration of the inhibitors, nature of metal, the mode of adsorption of the inhibitors and surface conditions. These compounds could be adsorbed in a flat orientation through the two oxygen atoms, one nitrogen atoms of the azo group and the type of groups in para position.

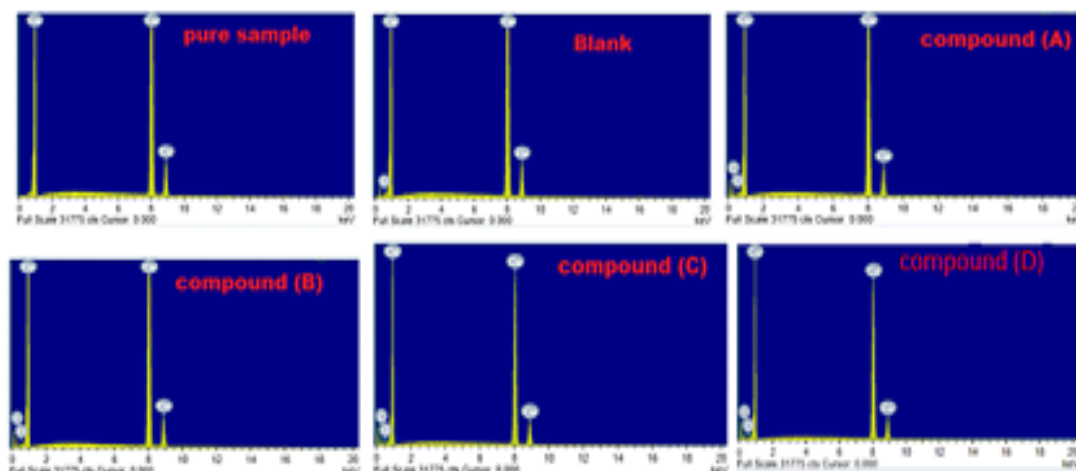


**Figure 13:** EDX analysis on copper in the absence and presence of  $30 \times 10^{-6}$  M of investigated compounds after 6 hours immersion at 25°C

**Table 13:** Surface composition (weight %) of copper after 6h of immersion in HNO<sub>3</sub> without and with the optimum concentrations of the studied inhibitors at 25°C

(Mass %)	Cu	C	O
Pure copper	100	--	--
Blank	94.83	--	5.17
Compound A	69.37	25.97	4.66
Compound B	73.34	23.48	3.18
Compound C	76.18	20.97	2.85
Compound D	78.26	20.12	1.62

It was concluded that the mode of adsorption depends on the affinity of the metal toward the  $\pi$ -electron clouds of the ring system [40]. Metals, such as Cu and Fe, which have a greater affinity toward aromatic moieties, were found to adsorb benzene rings in a flat orientation. Thus, it is reasonable to assume that the tested inhibitors were adsorbed in a flat orientation through the N- and O-atoms. In addition, there was decrease in inhibition efficiency with rise in temperature and the order of decreasing the inhibition efficiency of the investigated compounds in 1 M HNO<sub>3</sub> solution was: A > B > C > D. This behavior could be rationalized on the basis of the structure-corrosion inhibition relationship of organic compounds. Linear free energy relationships (LFERs) have been used to correlate corrosion rate in the absence and presence of the investigated compounds with their Hammett constituent constants ( $\sigma$ ) giving indication for inhibition efficiency order. The LFER or Hammett relations [41] are given by:

$$\text{Log} (k_{\text{rate of corr}}/k^{\circ}_{\text{rate of corr}}) = - \rho \sigma \quad (13)$$

Where  $k^{\circ}$  and  $k$  are the corrosion rates in the absence and presence of inhibitor, respectively.  $\rho$  is the reaction constant  $\sigma$  is the constituent in para-position, Thus, ( $\rho$ ) is a relative measure of the electron density at the reaction center. The constituents'  $\sigma$  who attract electrons from the reaction center (electron withdrawing groups) are assigned positive values, but electron donating groups which have negative values. Plot of Log (rate) vs.  $\sigma$  and the slope is  $\rho$  and its sign indicates whether the process is inhibited by an increase or decrease of the electron density at the reaction center. The magnitude of  $\rho$  indicates the relative sensitivity of the inhibition process to electronic effects. Figure 14 shows that the investigated compounds give a good correlation with correlation coefficient ( $R^2$ ) (0.929).

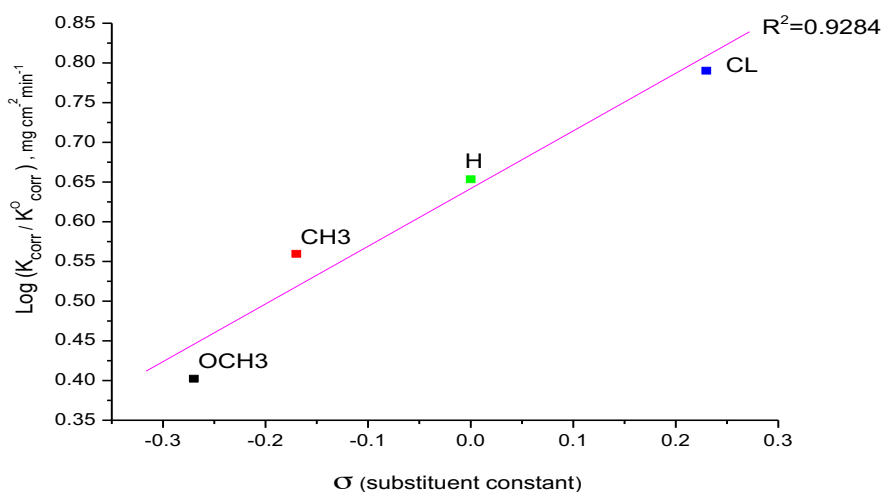


**Figure 14:** Relation between Logk, corrosion rate vs.  $\sigma$  (Hammett constants) of the substituent of investigated compounds

The large positive slope of the correlation line ( $\sigma = 0.726$ ) shows a strong dependence of the adsorption character of the reaction center on the electron density of the ring, with electron releasing substituent increasing the inhibition. This is because, in this type of derivatives, the center of adsorption is conjugated to the ring. Compound (A) has the highest percentage inhibition efficiency, this being due to the presence of p-OCH<sub>3</sub> group which is an electron donating group with negative Hammett constant ( $\sigma_{\text{pCH}_3} = -0.27$ ); this group would have increased the electron charge density on the molecule and might have add an additional center of adsorption to the molecule. Compound (B) comes after compound (A); this is due to the presence of p-CH<sub>3</sub> group which is an electron-donating group with Hammett constant ( $\sigma_{\text{CH}_3} = -0.17$ ), Also this group would have increased the electron charge density on the molecule but with lesser amount than p-OCH<sub>3</sub> group in compound (A). Compound (C) with Hammett constant ( $\sigma_{\text{H}} = 0.0$ ) comes after compound (B) in percentage of inhibition efficiency, because H-atom in para position has no effect on the charge density on the molecule. Finally, compound (D) is the lowest in percentage inhibition efficiencies. This is due to the presence of p-Cl group which being electron withdrawing group with positive Hammett constants ( $\sigma_{\text{Cl}} = +0.23$ ), and depends on the magnitude of their withdrawing character.

## Conclusions

- 1- All the investigated compounds are good corrosion inhibitors for copper in 1 M HNO<sub>3</sub> solutions, the effectiveness of these inhibitors depends on their structures and the variation in inhibitive efficiency depends on the type and the nature of the substituent present in the inhibitor molecules.
- 2- The adsorption of inhibitors depends on its concentration, temperatures and the nature of the inhibitor and metal.
- 3- EFM can be used as a rapid and nondestructive technique for corrosion measurements without prior knowledge of Tafel slopes.
- 4- The results of EIS revealed that an increase in the charge transfer resistance and a decrease in double layer capacitances when the inhibitor is added and hence an increase in % IE. This is attributed to increase of the thickness of the electrical double layer.
- 5- Results obtained from potentiodynamic polarization indicated that the investigated derivatives are mixed-type inhibitors.
- 6- The adsorption of all investigated compounds on copper surface obeys the Temkin adsorption isotherm model and the type of adsorption is mixed adsorption.
- 7- SEM-EDX images and analyses obtained in the presence of these compounds revealed the formation of thin film on the surface of copper.
- 8- The results obtained from chemical and electrochemical measurements were in good agreement. The order of % IE of these investigated compounds is in the following order:

Compound (A) > Compound (B) > Compound (C) > Compound (D)

## References

1. Crundwell F.K., *Electrochim. Acta*, 37 (1992) 2101.
2. Dafli A., Hammouti B., Mokhlisse R., Kertit S., *Corros. Sci.*, 45 (2003) 1619.
3. Mihit M., Bazzi L., Salghi R., Hammouti B., Ellssami S., AitAddi E., *Int. sci. J. Alternative Energy and Ecology*, 62 (2008).
4. Sherif E. M., Su-Moon Park, *Corros.Sci.*, 48 (2006) 4065.
5. Stupnisek-Lisac E., Brnada A. and Maance A.D., *Corros.Sci.*, 42 (2000) 243.
6. Moretti G. and Guidi F., *Corros.Sci.*, 44 (2002) 1995.
7. Smialowska- Szklarska Z., Kaminski M., *Corros. Sci.*, 13 (1973) 1.
8. Gomma G.K. and Wahdan M.H., *Bull. Chem. Soc. Jpn.*, 67(1994) 2621–2626.
9. Shoair A. G. F., (2007), *Journal of Coordination Chemistry*, 60(10) ( 2007) 1101.
10. Ma H., Chen S., Niu L., Zhao S., Li S., Li D., *J. Appl. Electrochem.*, 32(2002) 65.
11. Bosch R. W., Hubrecht J., Bogaerts W. F., Syrett B. C., *Corrosion*, 57 (2001) 60.
12. Abdel-Rehim S. S., Khaled K. F., Abd-Elshafi N. S., *Electrochim. Acta*, 51 (2006) 3269.
13. Muller A., Stockel W., *J. Electroanal. Chem.*, 219 (1987) 311.
14. Smyrl W.H., Bockris J.O.M., Conway B.E., Yeager E., White R.E. (Eds.), *Comprehensive Treatise of Electrochemistry*, Plenum Press, New York, 4(1981) 116.
15. El Achouri M., Kertit S., Gouttaya H.M., Nciri B., Bensouda Y., PereM L., Infante R., Elkacemi K., *Prog. Org. Coat.*, 43 (2001) 267.
16. Macdonald J.R., Johanson W.B., Macdonald J.R. (Ed.), John Wiley & Sons, New York, (1987).
17. Mertens S. F., Xhoffer C., Decooman B. C., Temmerman E., *Corrosion*, 53 (1997) 381.
18. Lagrenee M., Mernari B., Bouanis M., Traisnel M. and Bentiss F., *Corros. Sci.*, 44 (2002) 573.
19. Bentiss, F.; Lagrenee, M.; Traisnel, M. *Corrosion*, 2000, 56(7), 733–742.
20. Kus E., Mansfeld F., *Corros. Sci.*, 48 (2006) 965.
21. Zhang D. Q., Cai Q. R., He X. M., Gao L. X., Kim G. S., *Mater. Chem. Phys.*, 114 (2009) 612-617.
22. TrabANELLI G., in “Corrosion Mechanisms” (Ed. F. Mansfeld) Marcel Dekker, New York, 119 (1987).
23. Fouda A. S., Abd. El-Aal A., Kandil A. B., *Desalination*, 201 (2006) 216.
24. Asaf F.H., Abou- Krishna M., Khodari M., EL-Cheihk F., Hussien A. A., *Mater. Chem.Phys.*, 93 (2002) 1.
25. Fiala A., Chibani A., Darchen A., Boulkamh A., Djebbar K., *Appl. Surf. Sci.*, 253 (2007) 9347.
26. Arab S.T. and Noor E.M., *Corrosion*, 49 (1993) 122.
27. Durnie W., Marco R.D., Jefferson A., Kinsella B., *J. Electrochem. Soc.*, 146 (1999) 1751.
28. Gomma M. K. and Wahdan M. H.; *Mater. Chem. Phys.*, 39 (1995) 209.
29. Khamis E., *Corrosion*, 46 (1990) 476.
30. Fouda A. S, El-desoky A.M., Nabih A., *Advances in Materials and Corrosion*, 2 (2013) 9.
31. Frumkin. A. N., *Zeitschrift fur Physikalische Chemie*, 116 (1925) 466.
32. El-Awady A., Abd El-Nabey B., Aziz G., *Electrochem.Soc.*, 139 (1992) 2149.
33. Tang L., Li X., Si Y., Mu G. and Liu G., *Mater. Chem. Phys.*, 4 95 (2006) 29.
34. Maayta A. K. and Al-Rawashdeh N. A. F., *Corros.Sci.*, 6 (2004) 1129.
35. Durnie W., Marco R D, Jefferson A. and Kinsella B., *J Electro chem. Soc.*, 146 (1999) 1751.
36. Fouda A. S., Mekkia D.A., Badr H., *Journal of the Korean Chemical Society*, 57 (2013) 2.
37. Li X. and Mu G., *Appl. Surf. Sci.*, 252 (2005) 1254.
38. Mu G., Li X. and Liu G., *Corros. Sci.*, 47 (2005) 1932.
39. Vajpeyi M., Gupta S., and Pandey G. N., *Corros. Prev. Control*, October (1985) 102.
40. Chauhan L.R. and Gunasekaran G., *Corros. Sci.*, 49 (2007) 1143–1161.
41. Ashassi-Sorkhabi H., Shaabani B., and Seifzadeh D., *Appl. Surf. Sci.*, 239 (2005) 154–164